Am J Transl Res 2020;12(5):1862-1872
www.ajtr.org /ISSN:1943-8141/AJTR0109110

Original Article

In vivo characterization of PD-L1 expression in breast cancer by immuno-PET with ^{89}Zr-labeled avelumab

Miao Li[1,2*], Emily B Ehlerding[2*], Dawei Jiang[2], Todd E Barnhart[2], Weiyu Chen[2], Tianye Cao[2], Jonathan W Engle[2], Weibo Cai[2]

[1]Department of Radiology, The First Affiliated Hospital of Xi'an Jiaotong University, 277 West Yanta Road, Xi'an 710061, Shaanxi, China; [2]Departments of Radiology and Medical Physics, University of Wisconsin-Madison, 1111 Highland Avenue, Madison 53705, Wisconsin, United States. [*]Equal contributors.

Received February 12, 2020; Accepted April 20, 2020; Epub May 15, 2020; Published May 30, 2020

Abstract: Programmed death protein 1 and programmed death-ligand 1 (PD-1/PD-L1) have been widely studied as one of the most critical immune check-point pairs in the cancer microenvironment. In breast cancer (BrCa), the expression of PD-L1 is regarded as a determinant biomarker for patient stratification and prediction of inhibition response. Quantitative positron emission tomography (PET) imaging of PD-L1 expression in tumors using a therapeutic antibody in the clinic seems to be a promising approach that can complement conventional histopathological methods and overcome several issues, such as the tumor heterogeneities, sampling representativeness and clear differentiation of positive and negative results. In this study, we synthesized and evaluated ^{89}Zr-labeled avelumab (Ave) for the in vivo characterization of PD-L1 expression in BrCa. Confocal imaging of BrCa cells and flow cytometry were employed to evaluate PD-L1 expression in MDA-MB-231 cells. The intact human monoclonal antibody targeting PD-L1, i.e., Ave, was conjugated to p-SCN-Deferoxamine (Df) and labeled with ^{89}Zr. After intravenous injection of ^{89}Zr-Df-avelumab (^{89}Zr-Df-Ave), PET imaging of MDA-MB-231 tumor-bearing mice, with or without blocking, was performed. High PD-L1 expression of MDA-MB-231 cells was confirmed by in vitro immuno-fluorescent staining and flow cytometry. PET imaging indicated the peak uptake of ^{89}Zr-Df-Ave in the tumor (6.4±1.0 %ID/g), spleen (10.2±0.7 %ID/g) and lymph nodes (6.9±1.0 %ID/g) at 48 h after injection (n=4). Blocking study using unlabeled Ave could reduce the tracer uptake in these tissues (5.2±1.0 %ID/g in the tumor, 4.9±0.5 %ID/g in the spleen and 5.8±1.1 %ID/g in lymph nodes at 48 h, n=4), which demonstrated the specificity of ^{89}Zr-Df-Ave. Biodistribution study and immuno-fluorescent staining were consistent with the quantitative data from PET imaging. Herein, we offer the evidence supporting the value of immuno-PET imaging using ^{89}Zr-Df-Ave for non-invasive characterization of PD-L1 expression in BrCa and the applicability of this tracer in BrCa for treatment evaluation after immunotherapy.

Keywords: Positron emission tomography, PD-L1, breast cancer, avelumab, zirconium-89

Introduction

In females, breast cancer (BrCa) is the most common type of newly-diagnosed cancer and the leading cause of consequent mortality (i.e., the top cause globally and the second in the United States) [1, 2]. The current standard-of-care treatment for BrCa is insufficient because of inherent or drug-induced resistance, which underpins metastasis, relapse, and even mortality.

The introduction of immune checkpoint blockade therapy has demonstrated promising efficacy and may address an unmet need in a new wave of precision medicine. Among the several checkpoints investigated by researchers, the programmed death protein 1 (PD-1) and programmed death-ligand 1 (PD-L1) have been widely interrogated as one of the most critical immune check-point pairs in the tumor microenvironment (TME). Unfortunately, not all the patients respond to the immune checkpoint blockade. Only less than 20% of the pretreated patients can receive benefit from standalone treatment with checkpoint inhibitors [3, 4]. Therefore, the development of biomarkers to guide patient selection, to assist with combinatorial therapy, and to predict on-treatment response is highly demanded [5, 6].

Biomarkers could potentially optimize outcomes, minimize adverse events, or the risk of toxicity, avoid unnecessary expense, and eventually improve patient care in immunotherapy. The most popular biomarker investigated clinically for immunotherapy is the expression of PD-L1 in the TME, which has been approved by the Food and Drug Administration (FDA) of the United States through several companion diagnostic tests. However, the reliability of the results from biopsies with conventional immunohistochemistry (IHC) is challenged by a few concerns: 1) The intra-tumoral and inter-lesional heterogeneity between primary foci and metastasis may cause focal expression of PD-L1 to be missed during sampling; 2) PD-L1 expression in the TME is dynamic and may alter after therapeutic intervention; however, biopsy is usually performed before drug administration, and it is impractical to be frequently repeated, so the real-time readout of biopsies is suboptimal; 3) The methodological parameters, including the pre-treatment handling of specimens, the epitope specificity/affinity of the staining antibody and the threshold of positivity, may vary between tests, which leads to poor uniformity in the determination of PD-L1 levels by different tests; 4) PD-L1 exists both on the surface and in the cytoplasm of tumor cells and tumor-associated immune cells, which hinders the identification of the expressing site by morphology [7, 8].

Compared with IHC, in vivo monitoring of PD-L1 expression via molecular imaging displays some distinct advantages: 1) It covers all the suspectable lesions at different anatomic sites comprehensively, including the primary/metastatic ones; 2) As a non-invasive approach, it allows repeating image acquisition, making surveillance during disease progression and intervention possible, which facilitates personalization in clinical management [9-11]. ImmunoPET is a popular choice for imaging PD-L1, via the labeling of PD-L1-specific agents with a radionuclide. The merits of immunoPET include: 1) High sensitivity; 2) Superior specificity towards targets; 3) Reproducible quantification; and 4) Only cell-surface markers are accessible by antibody tracers [12, 13].

Several immunoPET tracers targeting PD-L1 have been reported in pre-clinical/clinical studies. One of the most practical options is the tracer derived from the antibodies available for treatment, e.g., Atezolizumab (Atz, MPDL-3280A), which has proven to be reliable in the assessment of PD-L1 expression in BrCa [14-16]. Apart from Atz, avelumab (MSB-0010718C; Ave) is another human IgG1 monoclonal antibody which newly emerges for targeting PD-L1. FDA approved Ave for the treatment of Merkel cell carcinoma and urothelial carcinoma. It is now under a phase I clinical trial for the therapy of several subtypes of BrCa [17, 18]. Ave has also been tested for the near-infrared photo-immunotherapy targeting PD-L1 in murine models of lung adenocarcinoma [19]. All these progress about Ave enhanced our confidence in the safety and feasibility of immunoPET imaging based on the tracer derived from Ave.

In this paper, we confirmed the high expression of PD-L1 in a classical human BrCa cell line in murine xenograft models, devised the [^{89}Zr]zirconium-labeled Ave as a tracer and finally validated the efficacy of this tracer for PET imaging. We aim to preliminarily evaluate the immunoPET biomarker for non-invasive monitoring of PD-L1 expression in BrCa.

Materials and methods

Chemicals

Ave (Bavencio®) was obtained from EMD Serono, Inc. (Rockland, MA). 1-(4-isothiocyanatophenyl)-3-[6,17-dihydroxy-7,10,18,21-tetraoxo-27-(N-acetylhydroxylamino)-6,11,17,22-tetraazaheptaeicosine] thiourea (p-SCN-deferoxamine or Df) was purchased from Macrocyclics, Inc. (Dallas, TX). AlexaFluor488™-labeled goat anti-human antibody was purchased from Invitrogen, Inc. (Eugene, OR). Pharmingen rat anti-mouse CD31 antibody was purchased from BD Bioscience, Inc. (San Diego, CA). Cy3-labeled donkey anti-rat antibody was purchased from Jackson, Inc. (West Grove, PA). Non-specific human IgG protein was purchased from Invitrogen, Inc. (Rockford, IL). PD-10 desalting columns were supplied by GE Healthcare, Inc. (Piscataway, NJ). 4',6-diamidino-2-phenylindole (DAPI) is the product of Vector Laboratories, Inc. (Burlingame, CA). Hoechst 33342 is provided by LifeTechnologies of ThermoFisher, Inc. (Eugene, OR). Matrigel was purchased from Corning, Inc. (Bedford, MA). Dulbecco Modified Eagle Medium (DMEM) was obtained from Gibco, Inc. (Grand Island, NY).

Fetal bovine serum (FBS) was provided by Gemini, Inc. (West Sacramento, CA). All other reagents were from ThermoFisher, Inc. (Fair Lawn, NJ).

Chelator conjugation and radiolabeling

Chelator reagent Df was dissolved in 15 μL of dimethyl-sulfoxide (DMSO), and Ave was dissolved in the mixture (500 μL) of 1× phosphate-buffered saline (PBS; pH 7.4)/$NaHCO_3$-Na_2CO_3 buffer (0.1 M, pH 9.2) (v/v=1:1). The Df and Ave were mixed (molar ratio=20:1). The mixture was incubated at room temperature (RT) for 2 h with constant shaking and later purified by PD-10 (PBS as the eluant). The fractions of Df-conjugated Ave (Df-Ave) products were merged, and the peak fraction of solute was confirmed on the NanoDrop One/One^C spectrophotometer (ThermoFisher; Waltham, MA).

An $^{89}Y(p,n)^{89}Zr$ reaction was performed in an onsite PETtrace cyclotron (GE Healthcare; Milwaukee, WI) to prepare ^{89}Zr. The target material [^{89}Y]yttrium foil (250 μm, 99.9% in purity) was bombarded by a 5 mA current of 16.4 MeV proton for 2 h. After bombardment, the foil was dissolved in concentrated HCl (Ultrex grade; Mallinckrodt; Dublin, Ireland), and the HCl solution was loaded onto a column packed with hydroxamate-functionalized resin as the sorbent. After the washing step with 6 N HCl, the ^{89}Zr was eluted by 1 M oxalic acid and collected. The final product of nuclide was the oxalic acid solution of ^{89}Zr oxalate.

The ^{89}Zr oxalate (60 MBq, 1.6 mCi) was added into 500 μL of HEPES buffer (0.5 M, pH 7.0). The pH value was adjusted to 7.0-7.5 by 1 M Na_2CO_3. Then 150 μg of Df-Ave was added into the HEPES buffer solution. The coordination reaction was undertaken at 37°C with constant shaking (800 rpm) for 1 h. The reaction solution was purified by PD-10 (PBS as the eluent). At last, the fractions of ^{89}Zr-Df-avelumab (^{89}Zr-Df-Ave) were combined and passed through 0.22 μm sterile filter for intravenous administration.

Cell culture

Human BrCa cell line MDA-MB-231 was provided by the American Type Culture Collection (ATCC; Manassas, VA). The cells were cultured in DMEM medium with high glucose and FBS (10%). The T75 flasks containing the cells were placed in a humidified constant thermo-incubator at 37°C with CO_2 (5%). When the confluence reached ~70%, cells were harvested for tumor inoculation and in vitro experiments.

Tumor model preparation

Cells suspended in cold PBS (4°C) were mixed with Matrigel in a ratio of 1:1 (v/v). Approximately 5×10^6 cells in 100 μL of the mixture were inoculated into the right hind-limb of each female athymic nude mouse (4-5 weeks in age; Envigo; Cambridge Shire, UK) subcutaneously with an insulin syringe pre-cooled on ice. The injection site was between the skin and muscle layers and ~10 mm from the spiking points on the limbs. The injected mixture can be adsorbed in 1-2 days. Tumors generally appeared at ~10 days post-inoculation. The growth of the tumor was monitored by palpation. At ~5 weeks post-inoculation, tumors with a diameter of ~10 mm were accepted for in vivo experiments.

Confocal imaging of cell line and flow cytometry

The PD-L1 expression on the MDA-MB-231 cells was validated by immuno-fluorescent staining and confocal imaging. The cells were cultured in glass-bottom dishes (Φ 50 mm, ~2×10^5 cells/dish) and grown at 37°C in CO_2 (5%) overnight. After blocking, cells were incubated with Ave (as primary antibody; 10 μg/mL) at RT for 45 min and goat anti-human secondary antibody at RT for 45 min in the dark. Then the cells were stained with Hoechst (5 μg/mL) at RT for 30 min in the dark and imaged on an A1R confocal microscope (Nikon, Inc.; Melville, NY).

PD-L1 expression on the tumor cell surface, along with the binding affinity of Df-Ave, was verified in the MDA-MB-231 cell line by flow cytometry. The cells were suspended in PBS (4°C; ~10^7 cells/mL) and split to aliquots of ~1.5×10^6 cells/tube. After blocking, the cells were incubated with PBS (4°C; as the control of blank cells), the goat anti-human secondary antibody (as the controls of secondary antibody only; 5 μg/mL), Ave, Df-Ave and IgG (all the last three as primary antibodies; 10 μg/mL) for 1 h in ice bath, respectively. The cells engaging with Ave, Df-Ave, and IgG were then

incubated with the goat anti-human secondary antibody (5 μg/mL) for 1 h on ice in darkness, respectively. Finally, all cells were re-suspended in 300 μL of PBS (4°C) for analysis on a 5-Laser LSR Fortessa cytometer (Becton-Dickinson, Inc.; San Jose, CA). Cell counts were recorded and analyzed using FlowJo (ver. X.0.7; Tree Star, Inc.; Ashland, OR) software.

PET imaging and biodistribution

All the animal studies follow the procedures in compliance with the regulations of the Institutional Animal Care and Use Committee (IACUC), University of Wisconsin-Madison (UW-Madison). An Inveon Micro-PET/CT scanner (Siemens Medical Solutions USA, Inc.) was employed for in vivo imaging. 6-9 MBq (0.16-0.24 mCi) of ^{89}Zr-Df-Ave were injected into the nude mice through the lateral tail vein. In the pre-blocking study, 1.5 mg of unlabeled (cold) Ave was injected to each mouse 24 h before the injection of ^{89}Zr-Df-Ave. The images were acquired by 5-15 min of static scanning at given time-points post-injection (p.i.) respectively. The region of interest (ROI) in major organs was delineated and the corresponding mean uptake was quantified in the percentage of injected dose per gram (%ID/g, decay-corrected) by Inveon Research Workshop (IRW) software (Siemens, Inc.). The %ID/g value was calculated by dividing tissue activity in MBq/g (converted from the ROI uptake) with total radioactive dose injected.

All the mice were anesthetized and sacrificed by CO_2 inhalation immediately after the PET acquisition at 120 h p.i. The blood, major organs, and tumors were collected and weighed. The radioactivity of all the blood and tissue samples was assayed on a Wizard 2480 automatic γ-counter (PerkinElmer, Inc.; Waltham, MA) and readouts were converted into %ID/g.

Histology

The immediately frozen tissues of tumor and organs were sliced (5 μm) in the Experimental Pathology Laboratory in the Carbone Cancer Center, UW-Madison. Tissue sections were fixed in cold acetone for 10 min and dried in air at RT for 3 min. Then the sections were blocked, followed by the staining with Ave as the primary antibody (10 μg/mL) overnight at 4°C and with the goat anti-rabbit secondary antibody at RT for 1 h. The adjacent sections of the tissue engaged with the rat anti-mouse CD31 (vascular endothelium biomarker) primary antibody (10 μg/mL) at 4°C overnight and the donkey anti-rat secondary antibody (5 μg/mL) at RT for 1 h. Coverslips were mounted with DAPI. Fluorescent imaging was implemented on the same A1R confocal microscope.

Statistical analysis

Quantitative data were presented as mean ± standard deviation (SD). Means were compared using Student's *t*-test. $P < 0.05$ was considered as statistically significant.

Results and discussion

Radiochemistry

Ave was successfully conjugated with Df and radiolabeled with Zr-89. The ^{89}Zr-labeling reaction provides a specific activity of 13.6±5.1 mCi/mg (503.2±188.7 MBq/mg) and radiochemical yield of > 80% in the final product of ^{89}Zr-Df-Ave tracer.

Confocal imaging of cell line and flow cytometry

As depicted in **Figure 1**, the nuclei of MBA-MB-231 cells were stained by Hoechst (blue channel). The PD-L1 on the cells was heavily stained by Ave and exhibited strong fluorescence (green channel), while the cells engaging with non-specific human IgG showed minimal green fluorescent signal. This contrast verifies the high expression of PD-L1 on the MDA-MB-231 cell line. In the results of flow cytometry, cells stained with Ave and Df-Ave shared notable positive shifts comparing with control groups, confirming the high expression of PD-L1 on the MDA-MB-231 cell surface. It also corroborates that the affinity of Ave to PD-L1 is not compromised by Df conjugation (**Figure 2**). The cells incubated with non-specific IgG also give unobservable shift (**Figure 2**). The shift in the IgG group of flow cytometry and the negative signal in the confocal images of the IgG group are the circumstantial evidence of the specificity of Ave and Df-Ave. All these in vitro results support that

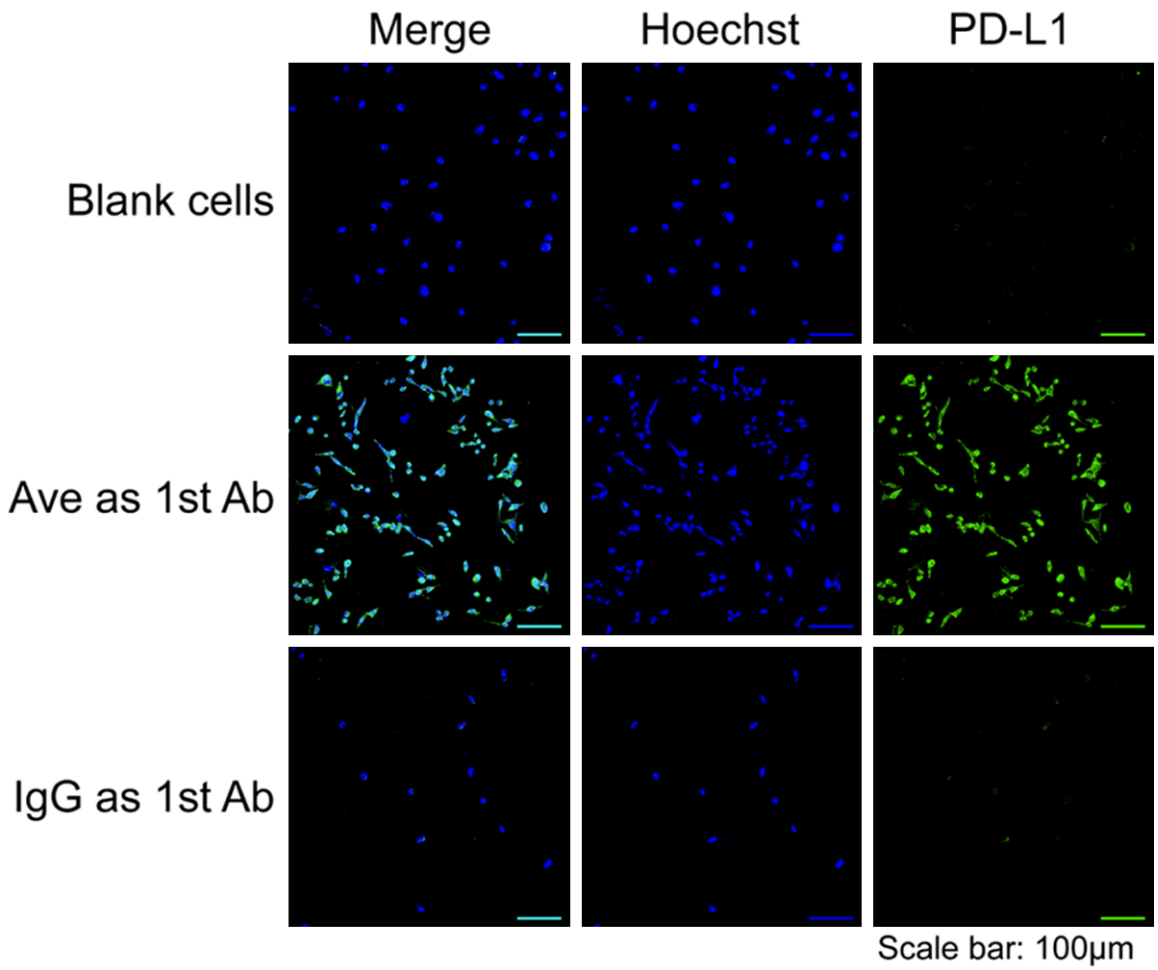

Figure 1. Confocal imaging of MDA-MB-231 breast cancer cell line after immunofluorescent staining. Sample groups: Hoechst, the nucleus stained by Hoechst; PD-L1, the PD-L1 expression; Ave as 1st Ab, the samples stained by avelumab as the primary antibody; IgG as 1st Ab, the samples stained by non-specific IgG as the primary antibody.

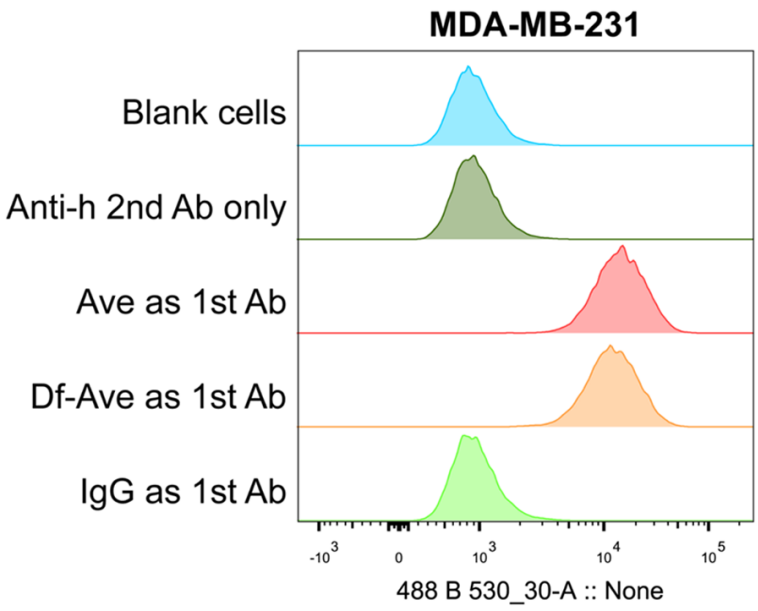

Figure 2. PD-L1 expression in the MDA-MB-231 breast cancer cell line measured by flow cytometry. Sample groups: Anti-h 2nd Ab only, the controls engaging with fluorescent goat anti-human secondary antibody only; Ave as 1st Ab, the samples engaging with avelumab as the primary antibody; Df-Ave as 1st Ab, the samples engaging with Df-avelumab as the primary antibody; IgG as 1st Ab, the samples engaging with non-specific IgG as the primary antibody. n=3.

the MDA-MB-231 cell line is a PD-L1 positive BrCa cell line and Df-Ave is a promising tracer for PD-L1 imaging in BrCa.

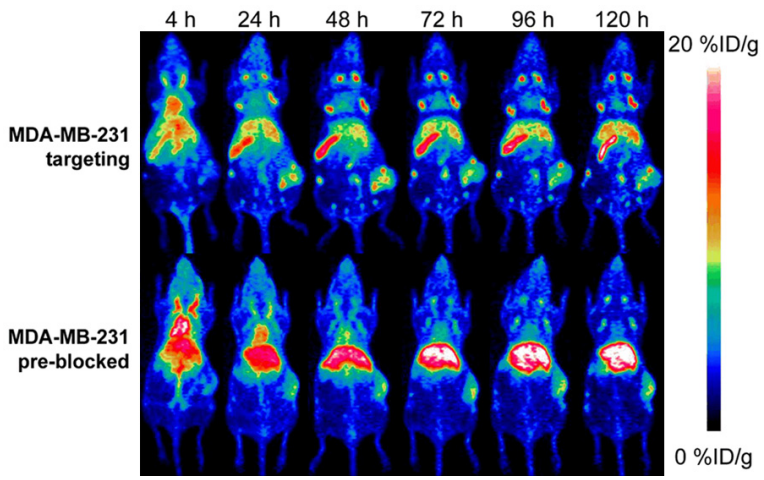

Figure 3. The typical positron emission tomography (PET) maximum-intensity projections (MIP) of MDA-MB-231 breast cancer model with/without pre-blocking.

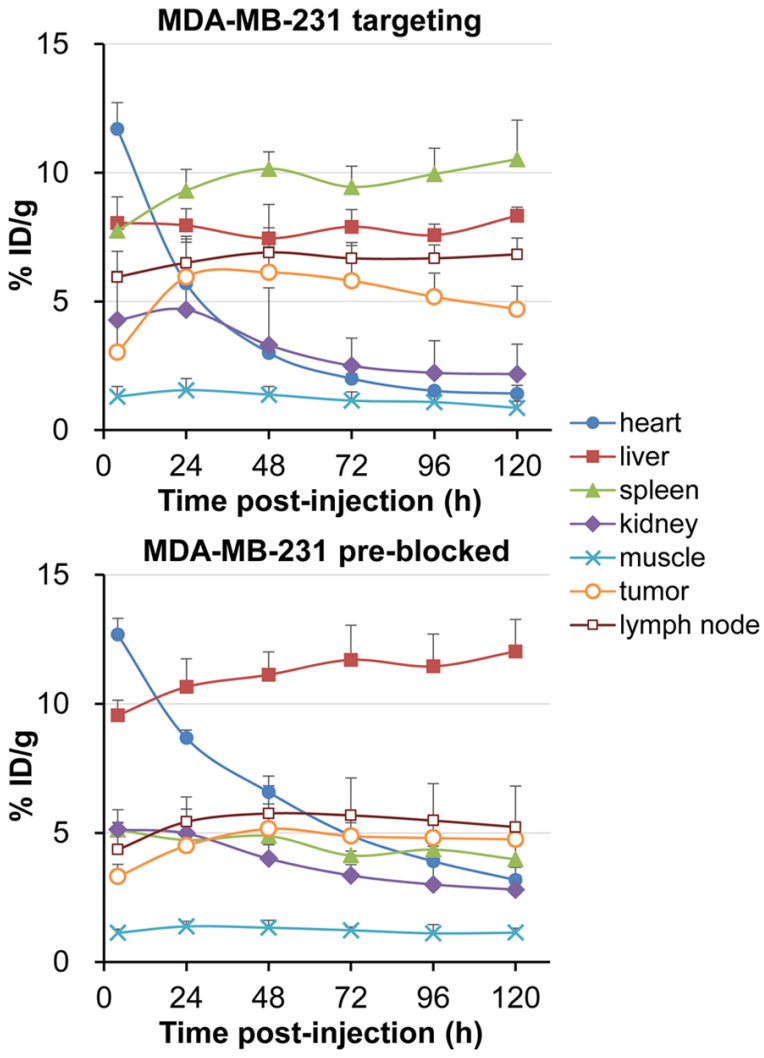

Figure 4. The uptake kinetics of the region of interest (ROI) in the positron emission tomography (PET) images of MDA-MB-231 breast cancer model with/without blocking, n=4. $P < 0.05$.

In vivo PET imaging and ex vivo biodistribution of ^{89}Zr-Df-Ave

Having confirmed the positive expression of PD-L1 on MDA-MB-231 cells, PET imaging was performed on tumor-bearing mice using Zr-89 labeled Ave and noticeable tumor uptake differences were found between the targeting and blocking groups at all time-points from 4 to 120 h p.i. (**Figure 3**), as well as the uptake kinetics of liver, spleen and lymph nodes (**Figure 4**, $P < 0.05$). Generally, the uptake in the tumors of the targeting model is slightly higher than that in the pre-blocked ones. ^{89}Zr-Df-Ave showed longer blood retention in the blocking group. ^{89}Zr-Df-Ave pre-blocked by the injection of 1.5 mg unlabeled (cold) Ave at 24 h before tracer administration translocates from spleen and lymph tissue to liver, in which its absorption by the reticuloendothelial system is non-selective and the primary route of metabolism of protein-based tracers.

Tracer accumulation of the tumor, major organs, and lymph nodes as measured by the ROI analysis are plotted in **Figure 4**. In the targeting group, the accumulation of ^{89}Zr-Df-Ave in tumors reaches a peak at 48 h p.i. Then it remains descending to the end of image acquisition (3.0±1.4, 6.0±1.6, 6.1±1.0, 5.8±1.4, 5.2±0.9, 4.7±0.9 %ID/g at 4, 24,

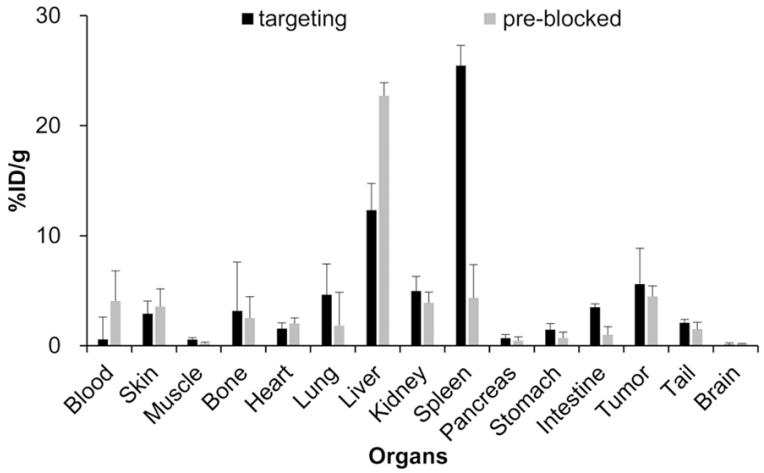

Figure 5. The radioactive ex vivo bio-distribution in the tumors and major organs of the MDA-MB-231 breast cancer model without/with blocking, n=4. $P < 0.05$.

48, 72, 96, 120 h p.i., respectively; n=4). In the pre-blocked group, the uptake of ^{89}Zr-Df-Ave in tumor grows more slowly and stays in a plateau from 48 h p.i. to 120 h p.i. (3.3±0.5, 4.5±0.6, 5.2±1.0, 4.9±0.8, 4.8±0.5, 4.8± 0.6 %ID/g at 4, 24, 48, 72, 96, 120 h p.i., respectively; n=4). The difference in the tumor uptake between the targeting and pre-blocking group at 48 h p.i. is found to be significant ($P < 0.05$). Although Ave is a human IgG1 antibody, it also targets murine PD-L1 and is able to carry out an anti-tumor response in the xenograft model of mouse tumors as reported elsewhere [20]. This may partially explain why there is pronounced reactivity concentration in the spleen and lymph node in the current model. Besides, the non-targeted accumulation of ^{89}Zr-Df-Ave between the targeting/pre-blocked models are close to each other, since the uptake in kidney and muscle between the two models have approximate kinetics during the whole imaging process (**Figure 4**).

We further performed a biodistribution study at 120 h p.i. (**Figure 5**).

Histology

Tumor, spleen, and lymph nodes were collected and frozen immediately for slicing and fixation. Confocal images of these tissues after immunofluorescent staining is shown in **Figure 6**. The fluorescence from PD-L1 (in green) is visible and overlays with the cell nuclei (in blue) in tumor, spleen and lymph node tissues. Almost no overlap is found between the vasculature (in red) and PD-L1 (in green). These immunohistological results confirmed the profile of PD-L1 expression and uptake of ^{89}Zr-Df-Ave in the tumor and lymph node tissues provided by the quantitative PET imaging/biodistribution studies.

The splenic PD-L1 expression level revealed by IHC is the lowest one among all tissues in **Figure 6**, which unmatches the uptake profile of ^{89}Zr-Df-Ave in these given tissues of the targeting group shown in the ROI kinetics. Except for targeting PD-L1, the deposition of ^{89}Zr-Df-Ave in the spleen can be attributed to the antibody-dependent cell-mediated cytotoxicity (ADCC) as well. Unlike another classical therapeutic monoclonal antibody against PDL1, i.e., Atz, Ave maintains its naive Fcγ domain [21]. Thus, the murine Fc receptor (FcγRI) may interact with exogenous Ave. This ADCC effect induced by Ave not only contribute to the killing of tumor cells but also accounts for its physiological uptake in the spleen to some extent [22].

PD-L1 as a responsive biomarker of cancer immunotherapy

The immuno-reaction in checkpoint-based tumor biology consists of three main steps: 1) T-cell-priming in lymphoid tissue; 2) The migration of T cells to the peripheral; 3) Anti-tumor action launched by activated effector cells in the TME. The blockade of the PD-1/PD-L1 pathway targets the last step which is a direct way to stimulate the cytotoxicity of $CD8^+$ T cells. PD-1/PD-L1 blockade is also a way with fewer side-effects, in comparison with the blockade of another key check-point CTLA-4 in the priming step. Thus, the PD-1/PD-L1 pathway becomes a more attractive target than CTLA-4 [7]. Because the patient with different molecular subtypes of breast cancers does not feedback similar effects to the treatment of PD-1/PD-L1 blockade, the exploration of an ideal biomarker for immunotherapy is highly necessary. It has been ob-

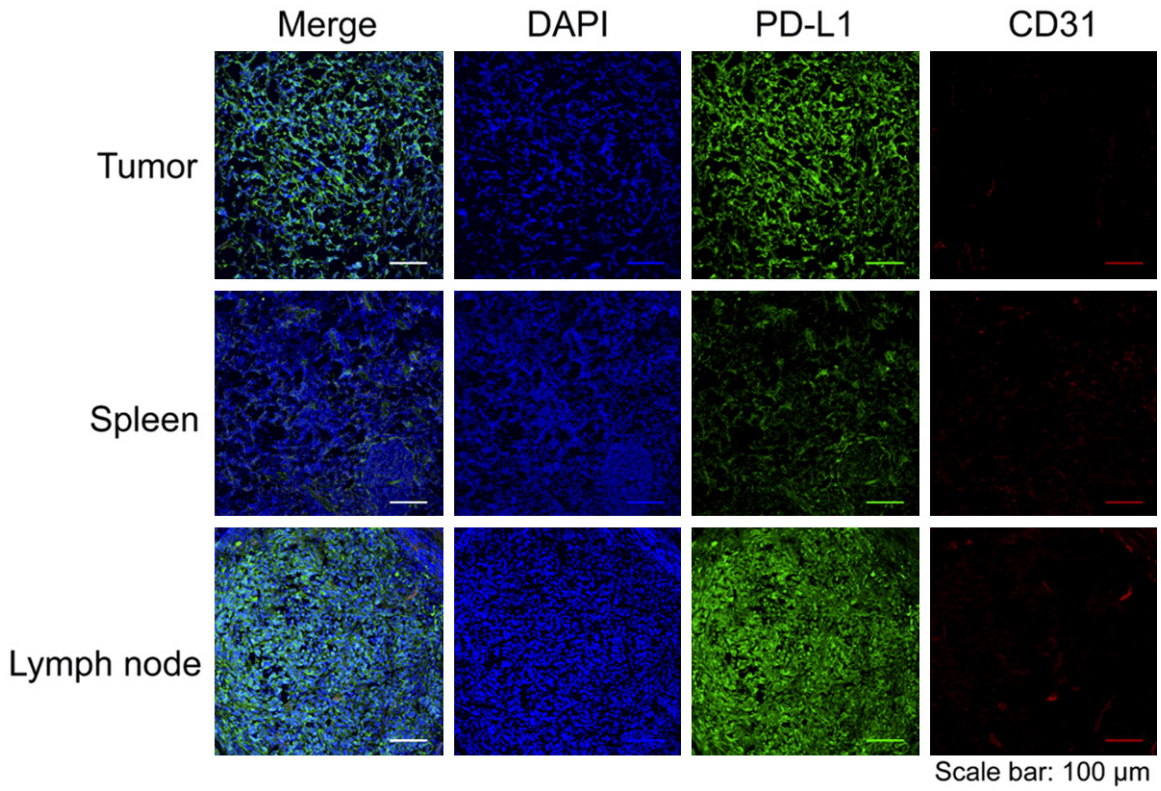

Figure 6. The confocal imaging of tumor, spleen, and lymph tissues from the MDA-MB-231 breast cancer model after immuno-fluorescent staining. Sample groups: DAPI, the nucleus stained by DAPI; PD-L1, the PD-L1 expression stained by avelumab as the primary antibody; CD31, the expression of vascular endothelium biomarker CD31.

served that a small subset of patients with negative PD-L1 expression also benefited from anti-PD-L1 agents. In other words, the opinion that PD-L1 expression alone serves as a predictor of responders is still controversial. Although this phenomenon raises questions against the utilization of PD-L1 as an absolute indicator for clinical decision-making, at least positive PD-L1 expression in the tumor could enhance the chance of therapeutic response and prolonged survival [3, 8, 17].

It should be noted that: 1) PD-L1 is expressed both on BrCa cells and tumor-infiltrated immune cells (e.g., macrophage). PET imaging targeting PD-L1 is unable to distinguish their separate expression levels, neither the constitutive/adaptive PD-L1 expression on tumor cells. Fortunately, PD-L1 expressed on the immune cells in the tumor is usually under the detection limit, so the uptake of Ave tracer in tumor predominantly reflects the PD-L1 expression on tumor cells [29]; 2) High PD-L1 expression is only part of the premises for therapeutic response. Adequate tumor-infiltrated T cells are also required [7, 34]; 3) The expressing level of PD-L1 is heterogenic in the several subtypes of BrCa, so the predictive value of PD-L1 expression in individual subtype varies [35, 36]. To robustly predict the therapeutic response, comprehensive consideration ranging from PD-L1 quantification, tumor-infiltrated lymphocytes, neo-antigenicity defined by tumor mutation burden to the molecular subtypes of BrCa would be more logical.

Systematic evaluation of ^{89}Zr-Df-Ave

So far, molecular imaging is the most practical approach to compensate for the limitations of IHC assay in the real-time monitoring of PD-L1 expression in TME. It not only follows the status of the immune system but also implies the general progression of the disease. This helps clinicians to decide whether to proceed with PD-1/PD-L1 blockade or to use the blockade as an aid to current therapies [11, 23]. The most popular radiographic modality of

the in vivo imaging of PD-L1 expression ever reported is the quantitative immunoPET with Atz tracer in the clinical setting [16]. Thus, immuno-PET using the tracer derived from another emerging therapeutic antibody, e.g., Ave, is also a rational option. The first Ave tracer for the characterization of PD-L1 expression in the preclinical model is the IR700DX-Ave tested in fluorescent imaging, but it is not dedicated to quantitative assessment [19]. As for the Ave PET tracer, ^{89}Zr-Df-Ave has been applied in the murine BrCa model reported by a brief abstract [24]. The clinical trial of ^{89}Zr-Df-Ave for non-small cell lung cancer (NSCLC) is currently in the stage of patient recruitment [25]. Our study is a systematic evaluation and a complement to previous preclinical studies.

In vivo competition between cold antibodies and their corresponding tracers

An existed research of ^{89}Zr-Df-Ave indicated that the uptakes in tumor, spleen and lymph nodes were 2.44±0.58 to 3.03±0.2, 29.90±7.58 to 60.41±6.23 and 16.68±3.26 to 27.03±5.38 %ID/g, respectively [27], which is lower than that of the tumor but much higher than those of spleen and lymph node in our results. The difference may be due to the variant levels of target expression between cell/animal strains [27]. The co-injection of unlabeled Ave was able to suppress the deposition of ^{89}Zr-Df-Ave in the spleen in a dose-dependent profile, but the effect of suppression in the lymph node and increased tracer delivery to tumor showed no dose-dependency. In our studies, the expected intratumoral heterogeneity in the distribution of ^{89}Zr-Df-Ave, as well as the elevated radioactive concentration in the blood pool and liver caused by pre-blocking using unlabeled Ave are found. Although all the results from our pre-blocking studies support the tissue specificity of the Ave tracer, unlike the case of ^{89}Zr-Df-Ave, the uptakes in tumor, spleen, and lymph node all reduce to some extent after pre-blocking [27].

In some previous reports, the authors claimed that spleen usually acts as a sink organ to the administrated PD-L1 tracers derived from antibodies [15, 26, 28]. Generally, after pre-blocking or co-injection, the decreasing amplitude of tracer uptake in the spleen is positively correlated with the doses of unlabeled counterparts introduced. The escalated tumor uptake is considered to be the consequence of competitive binding, which releases more tracers available to engage with tumor tissue [29]. However, there are some counterexamples for this explanation. In these cases, the competition by the unlabeled counterparts overwhelms the affinity interaction of released tracers with PD-L1 in the tumor, leading to a decline in tumor uptake [30-33]. It was not only demonstrated in an immuno-competent murine model [32] but also corroborated by a single tracer in both immunocompetent and immuno-deficient mouse models [30]. It implies that the descending uptake in the tumor during blocking studies cannot be correlated to the status of immune function. Therefore, the effect on the biodistribution of antibody tracers targeting PD-L1 by blocking strategy using their unlabeled counterparts should not be merely generalized in imaging context. The manner of blocking (pre-blocking or co-injection), the dose of unlabeled counterparts, the timing of blocking and the exact way of impact on biodistribution kinetics to those tracers targeting PD-L1 need to be clarified in further systematic research.

The accumulation of Ave tracers in mouse lymphoid organs can be attributed to cross-reactivity between species [20]. Albeit the interspecies selectivity of the Ave tracers is not perfect, such cross-reactivity may be useful to guide the evaluation of immune response in an immunocompetent model for translational development [26].

Conclusion

Herein, PET imaging with ^{89}Zr-Df-Ave has been proved to be valuable in the in vivo assessment of PD-L1 expression in BrCa. The specific accumulation of ^{89}Zr-Df-Ave in a preclinical BrCa model was also validated by pre-blocking in the in vivo imaging and ex vivo biodistribution studies. All these results confirm the feasibility of immuno-PET with ^{89}Zr-Df-Ave targeting PD-L1 and may offer guiding information to the translation of Ave-derived tracers for patient stratification, therapeutic monitoring and response prediction in the checkpoint blockade treatment against BrCa.

Acknowledgements

This work was supported, in part, by the University of Wisconsin-Madison, the National Institutes of Health (P30CA014520) and the

National Natural Science Foundation of China (Program for Young Scholars, Grant No. 81703468).

Disclosure of conflict of interest

None.

Address correspondence to: Dr. Dawei Jiang, Department of Radiology, University of Wisconsin-Madison, Wisconsin, United States. Tel: 608-504-1696; E-mail: djiang29@wisc.edu; Dr. Weibo Cai, Departments of Radiology and Medical Physics, University of Wisconsin-Madison, Wisconsin, United States. Tel: 608-262-1749; E-mail: wcai@uwhealth.org

References

[1] Siegel RL, Miller KD and Jemal A. Cancer statistics, 2019. CA Cancer J Clin 2019; 69: 7-34.

[2] Winters S, Martin C, Murphy D and Shokar NK. Breast cancer epidemiology, prevention, and screening. In: Lakshmanaswamy R, editor. Progress in Molecular Biology and Translational Science: Elsevier; 2017. pp. 1-32.

[3] Lyons TG, Dickler MN and Comen EE. Checkpoint inhibitors in the treatment of breast cancer. Curr Oncol Rep 2018; 20: 51.

[4] Emens LA. Breast cancer immunotherapy: facts and hopes. Clin Cancer Res 2018; 24: 511-520.

[5] Polk A, Svane I, Andersson M and Nielsen D. Checkpoint inhibitors in breast cancer-Current status. Cancer Treat Rev 2018; 63: 122-134.

[6] Solinas C, Gombos A, Latifyan S, Piccart-Gebhart M, Kok M and Buisseret L. Targeting immune checkpoints in breast cancer: an update of early results. ESMO Open 2017; 2: 1-14.

[7] Topalian SL, Taube JM, Anders RA and Pardoll DM. Mechanism-driven biomarkers to guide immune checkpoint blockade in cancer therapy. Nat Rev Cancer 2016; 16: 275-287.

[8] Gibney GT, Weiner LM and Atkins MB. Predictive biomarkers for checkpoint inhibitor-based immunotherapy. Lancet Oncol 2016; 17: e542-e551.

[9] Vaz SC, Capacho AS, Oliveira FP, Gil N, Teixeira Barros C, Parreira A and Costa DC. Radiopharmacology and molecular imaging of PD-L1 expression in cancer. Clinical and Translational Imaging 2018; 6: 429-439.

[10] Marciscano AE and Thorek DLJ. Role of noninvasive molecular imaging in determining response. Adv Radiat Oncol 2018; 3: 534-547.

[11] Broos K, Lecocq U, Raes G, Devoogdt N, Keyaerts M and Breckpot K. Noninvasive imaging of the PD-1: PD-L1 immune checkpoint: embracing nuclear medicine for the benefit of personalized immunotherapy. Theranostics 2018; 8: 3559-3570.

[12] Nishino M, Ramaiya NH, Hatabu H and Hodi FS. Monitoring immune-checkpoint blockade: response evaluation and biomarker development. Nat Rev Clin Oncol 2017; 14: 655-668.

[13] Teng F, Meng X, Kong L and Yu J. Progress and challenges of predictive biomarkers of anti PD-1/PD-L1 immunotherapy: a systematic review. Cancer Lett 2018; 414: 166-173.

[14] Lesniak WG, Chatterjee S, Gabrielson M, Lisok A, Wharram B, Pomper MG and Nimmagadda S. PD-L1 Detection in tumors using [64Cu] Atezolizumab with PET. Bioconjugate Chem 2016; 27: 2103-2110.

[15] Moroz A, Lee C, Wang Y, Hsiao JC, Sevillano N, Truillet C, Craik CS, Fong L, Wang C and Evans MJ. A preclinical assessment of 89Zr-Atezolizumab identifies a requirement for carrier added formulations not observed with 89Zr-C4. Bioconjugate Chem 2018; 29: 3476-3482.

[16] Bensch F, van der Veen EL, Lub-de Hooge MN, Jorritsma-Smit A, Boellaard R, Kok IC, Oosting SF, Schröder CP, Hiltermann TJN, van der Wekken AJ, Groen HJM, Kwee TC, Elias SG, Gietema JA, Bohorquez SS, de Crespigny A, Williams SP, Mancao C, Brouwers AH, Fine BM and de Vries EGE. 89Zr-atezolizumab imaging as a non-invasive approach to assess clinical response to PD-L1 blockade in cancer. Nat Med 2018; 24: 1852-1858.

[17] Force J, Leal JHS and McArthur HL. Checkpoint blockade strategies in the treatment of breast cancer: where we are and where we are heading. Curr Treat Options Oncol 2019; 20: 35.

[18] Dirix LY, Takacs I, Jerusalem G, Nikolinakos P, Arkenau H, Forero-Torres A, Boccia R, Lippman ME, Somer R, Smakal M, Emens LA, Hrinczenko B, Edenfield W, Gurtler J, von Heydebreck A, Grote HJ, Chin K and Hamilton EP. Avelumab, an anti-PD-L1 antibody, in patients with locally advanced or metastatic breast cancer: a phase 1b JAVELIN solid tumor study. Breast Cancer Res Treat 2018; 167: 671-686.

[19] Nagaya T, Nakamura Y, Sato K, Harada T, Choyke PL, Hodge JW, Schlom J and Kobayashi H. Near infrared photoimmunotherapy with avelumab, an anti-programmed death-ligand 1 (PD-L1) antibody. Oncotarget 2017; 8: 8807-8817.

[20] Vandeveer AJ, Fallon JK, Tighe R, Sabzevari H, Schlom J and Greiner JW. Systemic immunotherapy of non-muscle invasive mouse bladder cancer with avelumab, an Anti-PD-L1 immune checkpoint inhibitor. Cancer Immunol Res 2016; 4: 452-462.

[21] Boyerinas B, Jochems C, Fantini M, Heery CR, Gulley JL, Tsang KY and Schlom J. Antibody-dependent cellular cytotoxicity activity of a novel anti-PD-L1 antibody avelumab (MSB0010718C) on human tumor cells. Cancer Immunol Res 2015; 3: 1148-1157.

[22] Vivier D, Sharma SK, Adumeau P, Rodriguez C, Fung K and Zeglis BM. The impact of FcγRI binding on immuno-PET. J Nucl Med 2019; 60: 1174-1182.

[23] Ehlerding EB, England CG, McNeel DG and Cai W. Molecular imaging of immunotherapy targets in cancer. J Nucl Med 2016; 57: 1487-1492.

[24] Jagoda EM, Vasalatiy O, Basuli F, Opina ACL, Williams MR, Wong K, Lane KC, Adler S, Ton AT, Szajek LP, Xu B, Butcher D, Edmondson EF, Swenson RE, Greiner J, Gulley J, Eary J and Choyke PL. Immuno-PET imaging of the programmed cell death-1 ligand (PD-L1) using the therapeutic mAb, avelumab. Mol Imaging 2019; 18: 1536012119829986.

[25] Herpe CV. PD-L1 imaging in non small cell lung cancer. 2018.

[26] Chatterjee S, Lesniak WG, Gabrielson M, Lisok A, Wharram B, Sysa-Shah P, Azad BB, Pomper MG and Nimmagadda S. A humanized antibody for imaging immune checkpoint ligand PD-L1 expression in tumors. Oncotarget 2016; 7: 10215-10227.

[27] Jagoda EM, Vasalatiy O, Basuli F, Opina ACL, Williams MR, Wong K, Lane KC, Adler S, Ton AT, Szajek LP, Xu B, Butcher D, Edmondson EF, Swenson RE, Greiner J, Gulley J, Eary J and Choyke PL. Immuno-PET imaging of the programmed cell death-1 Ligand (PD-L1) using a zirconium-89 labeled therapeutic antibody, avelumab. Mol Imaging 2019; 18: 1329205790.

[28] Nedrow JR, Josefsson A, Park S, Ranka S, Roy S and Sgouros G. Imaging of programmed cell death ligand 1: impact of protein concentration on distribution of anti-PD-L1 SPECT agents in an immunocompetent murine model of melanoma. J Nucl Med 2017; 58: 1560-1566.

[29] Wierstra P, Sandker G, Aarntzen E, Gotthardt M, Adema G, Bussink J, Raavé R and Heskamp S. Tracers for non-invasive radionuclide imaging of immune checkpoint expression in cancer. EJNMMI Radiopharm Chem 2019; 4: 29.

[30] Truillet C, Oh HLJ, Yeo SP, Lee C, Huynh LT, Wei J, Parker MFL, Blakely C, Sevillano N, Wang Y, Shen YS, Olivas V, Jami KM, Moroz A, Jego B, Jaumain E, Fong L, Craik CS, Chang AJ, Bivona TG, Wang C and Evans MJ. Imaging PD-L1 expression with immunoPET. Bioconjugate Chem 2018; 29: 96-103.

[31] Li D, Cheng S, Zou S, Zhu D, Zhu T, Wang P and Zhu X. Immuno-PET imaging of 89Zr labeled anti-PD-L1 domain antibody. Mol Pharmaceut 2018; 15: 1674-1681.

[32] Josefsson A, Nedrow JR, Park S, Banerjee SR, Rittenbach A, Jammes F, Tsui B and Sgouros G. Imaging, biodistribution, and dosimetry of radionuclide-labeled PD-L1 antibody in an immunocompetent mouse model of breast cancer. Cancer Res 2016; 76: 472.

[33] Donnelly DJ, Smith RA, Morin P, Lipovšek D, Gokemeijer J, Cohen D, Lafont V, Tran T, Cole EL, Wright M, Kim J, Pena A, Kukral D, Dischino DD, Chow P, Gan J, Adelakun O, Wang X, Cao K, Leung D, Bonacorsi SJ and Hayes W. Synthesis and biologic evaluation of a novel 18F-labeled adnectin as a PET radioligand for imaging PD-L1 expression. J Nucl Med 2018; 59: 529-535.

[34] Ribas A and Wolchok JD. Cancer immunotherapy using checkpoint blockade. Science 2018; 359: 1350-1355.

[35] Voutsadakis IA. Immune blockade inhibition in breast cancer. Anticancer Res 2016; 36: 5607-5622.

[36] Bertucci F and Gonçalves A. Immunotherapy in breast cancer: the emerging role of PD-1 and PD-L1. Curr Oncol Rep 2017; 19: 64.